Multilevel Deep Learning Network for County-Level Corn Yield Estimation in the U.S. Corn Belt

Jie Sun, Zulong Lai, Liping Di, *Senior Member, IEEE*, Ziheng Sun, Jianbin Tao, and Yonglin Shen

***Abstract*—Accurate and timely estimation of crop yield at a small scale is of great significance to food security and harvest management. Recent studies have proven remote sensing is an efficient method for yield estimation and machine learning, especially deep learning, can infer a good prediction by integrating multisource datasets such as satellite data, climate data, soil data, and so on. However, there are some bottleneck challenges to improve accuracy. First, the popular remote sensing data used for yield prediction fall into two major groups—time-series data and constant data. Surprisingly little attention has been devoted to deep learning networks which can integrate the two kinds of data effectively; second, both temporal and spatial features play a role in affecting the yields. But most of the existing approaches employed either convolutional neural network (CNN) or recurrent neural network (RNN). CNN cannot learn temporal patterns, while RNN barely can learn spatial characteristics. This work proposed a novel multilevel deep learning model coupling RNN and CNN to extract both spatial and temporal features. The inputs include both time-series remote sensing data, soil property data, and the model outputs yield. We experimented with the model in U.S. Corn Belt states, and used it to predict corn yield from 2013 to 2016 at the county-level. The results approve the effectiveness and advantages of the proposed approach over the other methods. In the future, the model will be used on other crops such as soybean and winter wheat to assist agricultural decision-making.**

***Index Terms*—Convolutional neural network (CNN), county-level, long short-term memory (LSTM), prediction, yield.**

I. Introduction

THE U.S. is the largest corn producer in the world. Corn accounts for more than 95% of total grain production in the U.S. The production of corn also plays a noteworthy role in the economy. However, the yield varies every year and is affected by natural disasters and socioeconomic reasons. To secure our food security, preventive adaptive policies should be made ahead of time to secure our food security and economy. Making preventive policies rely on information and yield prediction is one of the most important pieces.

Researchers often use either weather/climate data, satellite remote sensing products, and soil property data or their combination for crop yield prediction at regional scales. The weather data and satellite data are time-series data while the soil property data are commonly considered as constant data that will not change much in the foreseeable future. Because of its advantages such as large scale, continuous, multispectral, low cost and long-term archive, remote sensing has become one of the most important tools for yield estimation [1]–[3]. Several long-running satellites have been widely used in the task. For example, the advanced very high-resolution radiometer (AVHRR) is the primary sensor on board the National Oceanic and Atmospheric Agency (NOAA) polar-orbiting satellites. AVHRR data have been collected continuously since 1981. Although the NOAA/AVHRR satellites were initially designed to observe the Earth's weather in the form of cloud patterns, further research on the sensors demonstrated that they could also be used for yield prediction [4], [5]. However, the coarse resolution and inadequate spectral information of the AVHRR data may cause unsatisfied precision. The Moderate Resolution Imaging Spectroradiometer (MODIS) is another long-living Earth observation dataset. The images are taken starting in 1999 by the NASA satellite Terra, and another satellite Aqua started to take the images from 2002 simultaneously. The images have 36 spectral bands whose wavelengths range from 0.4 to 14.4 μm and have various spatial resolutions (2 bands at 250 m, 5 bands at 500 m, and 29 bands at 1 km). The two satellites image the entire Earth every 1 to 2 days. Because of its better spatial resolution, spectral response, and temporal resolution, MODIS is more suitable for crop growth monitoring and has been very popular in the yield prediction studies [6]–[8]. The Landsat program is the longest-running enterprise for the acquisition of satellite imagery of Earth. The Landsat data have improved spatial resolutions ranging from 15 to 60 m. However, its temporal resolution of 16 days may omit important observations within a typical growing season, particularly coupled with the effects of clouds [9].

Regardless of the kinds of satellite data being employed, most of the previous researchers prefer to build the relationship between some crop-related indexes and crop yield. The most used indexes extracted from raw satellite data include normalized difference vegetation index, enhanced vegetation index, green chlorophyll vegetation index, sun-induced chlorophyll fluorescence, and the fraction of absorbed photosynthetically active radiation, etc. [10]–[12]. These indexes are essentially

Manuscript received June 3, 2020; revised July 24, 2020 and August 12, 2020; accepted August 14, 2020. Date of publication August 25, 2020; date of current version September 16, 2020. The work was supported by the National Natural Science Foundation of China under Grant 41971371. *(Corresponding author: Zulong Lai.)*

Jie Sun, Zulong Lai, and Yonglin Shen are with the School of Geography and Information Engineering, China University of Geosciences, Wuhan 430074, China (e-mail: jiesun@cug.edu.cn; laizulong@cug.edu.cn; shenyl@cug.edu.cn).

Liping Di and Ziheng Sun are with the Center for Spatial Information Science and Systems, George Mason University, Fairfax, VA 22030 USA (e-mail: ldi@gmu.edu; zsun@gmu.edu).

Jianbin Tao is with the Department of Geographic Information Sciences, Central China Normal University, Wuhan 430079, China (e-mail: taojb@mail.ccnu.edu.cn).

Digital Object Identifier 10.1109/JSTARS.2020.3019046

multispectral reduction products, which can raise the efficiency but may cause information loss. Besides, weather data (e.g., land surface temperature (LST), precipitation, and vapor) and soil properties (e.g., clay content, organic carbon content, and PH) have been also included as input for yield prediction [13]. It appears that comprehensive factors can simulate the real growth condition of crops more accurately to improve the performance of yield prediction [14].

Machine learning (ML) have shown superior performance on various challenging tasks such as image classification, face recognition, parameter regression, and natural language processing by learning the complex features and correlations from a big training dataset [15], [16]. Recent studies have explored its use on yield prediction. Everingham *et al.* [17] found that the random forest (RF) model is quite good at predicting sugarcane yields in the early season. Ruβ found that support vector regression can serve as a better reference model for yield prediction than multilayer perceptron or regression tree (RT) [18]. With the development of artificial intelligence (AI), artificial neural networks (ANNs) have been tested on several different crops for yield prediction [5], [14], [19]–[23], and the results reflect that the ML methods can outperform the traditional regression methods. Kim *et al.* [24] compared several AI models for crop yield modeling, these models include multivariate adaptive regression splines, support vector machine, RF, extremely randomized trees, ANN, and deep neural network (DNN); the results suggested that the DNN with multiple hidden layers are more powerful to reveal the fundamental nonlinear relationship between predictors and yields. Khaki *et al.* designed a DNN for maize yield prediction in the 2018 Syngenta Crop Challenge. The results also confirmed that the DNN significantly outperformed other popular methods such as Lasso, shallow neural networks, and RT. Besides, the result revealed that environmental factors have a greater effect on the crop yield than genotype [25].

Recently, convolutional neural networks (CNN) and recurrent neural networks (RNN), two popular types of DNN [26], have attracted a lot of attention for yield prediction. Jiang *et al.* first employed long short-term memory (LSTM) for corn yield prediction. LSTM is a special form of RNN method, it is developed to seize the vanishing gradient problem encountered in RNN. The empirical results from county-level data in Iowa show that LSTM is efficient in time-series prediction with complex inner relations, which makes it suitable for yield prediction [27]. You *et al.* [28] employed CNN and LSTM for soybean yield prediction in the U.S., the results proved that CNN and LSTM can outperform traditional methods such as ridge regression and decision tree, furthermore, the performance of CNN is better than LSTM. Based on the work in [28], Wang *et al.* [29] showed promising results in predicting soybean crop yields in Argentina, they also achieved satisfactory results with a transfer learning approach to predict Brazil soybean harvests with a smaller amount of data. Russello proposed a novel 3-D CNN model for crop yield prediction task that leverages the spatio-temporal features, the results significantly outperform competitive state-of-the-art ML methods [30]. Yang *et al.* proposed a CNN-based model for rice yield prediction with low-altitude remotely sensed imagery. The very high spatial resolution imagery and multispectral datasets perform much better than the VIs-based regression model for rice grain yield estimation at the ripening stage [31]. It is well established that CNN can learn to recognize patterns across space while RNN is useful for solving temporal data problems. However, several limitations still exist. First, most of the previous researches only employed CNN or RNN independently. Hence, these methods cannot fully take advantage of CNN and RNN simultaneously. Second, most of these methods preferred employing averages of each band over a region as the features, leading to spatial information loss. Yet DL methods can learn rich features from the natural data instead of given limited handcrafted features, and then contribute to better results. It is important to keep the information on natural data as much as possible. Based on our knowledge, no previous research integrated time-series data, constant data, and deep learning for yield prediction yet.

This study used a combination of satellite data, weather data, and soil property data to predict corn yield in the U.S. Corn Belt from 2013 to 2016 at the county-level. A new composite DL model was proposed to take advantage of both CNN and RNN. The multilevel deep learning network (MLDL-Net) framework has two modules. The first module has two steps. The first step is using CNN to extract spatial features from MODIS imagery data and weather data. The second step is using LSTM to extract temporal features from time-series data. The second module is using CNN to extract features from soil property data. To automatically select effective features rather than hand-picking, a histogram-based method was involved to transform natural remote sensing data into fixed-bins histograms and use them to determine which features will be used as inputs. The output from the two modules will be put together as inputs into the final yield prediction step. Validation experiments have been done on the data of the U.S. Corn Belt. The main aims of the work are: 1) evaluate the performance of the proposed method for corn yield prediction in the U.S. Corn Belt; and 2) evaluate the influence of different data in the prediction task.

II. Materials And Methods

A. Study Area

In this study, the counties in the U.S. Corn Belt were selected as the study area. There are 13 states in the U.S. Corn Belt including North Dakota, South Dakota, Nebraska, Kansas, Minnesota, Iowa, Wisconsin, Illinois, Michigan, Indiana, Ohio, Kentucky, and Missouri, about 1175 counties in total. Fig. 1 shows the selected counties in the GEE.

B. Data

Considering the related impact factors, i.e., the data availability and generalizability of models, this study uses MODIS surface reflectance (SR) data, MODIS LST data, and Daymet weather data as the time-series data. The openlandmap data were selected as constant soil property data. These data can also fall into two categories, the one is phenological information

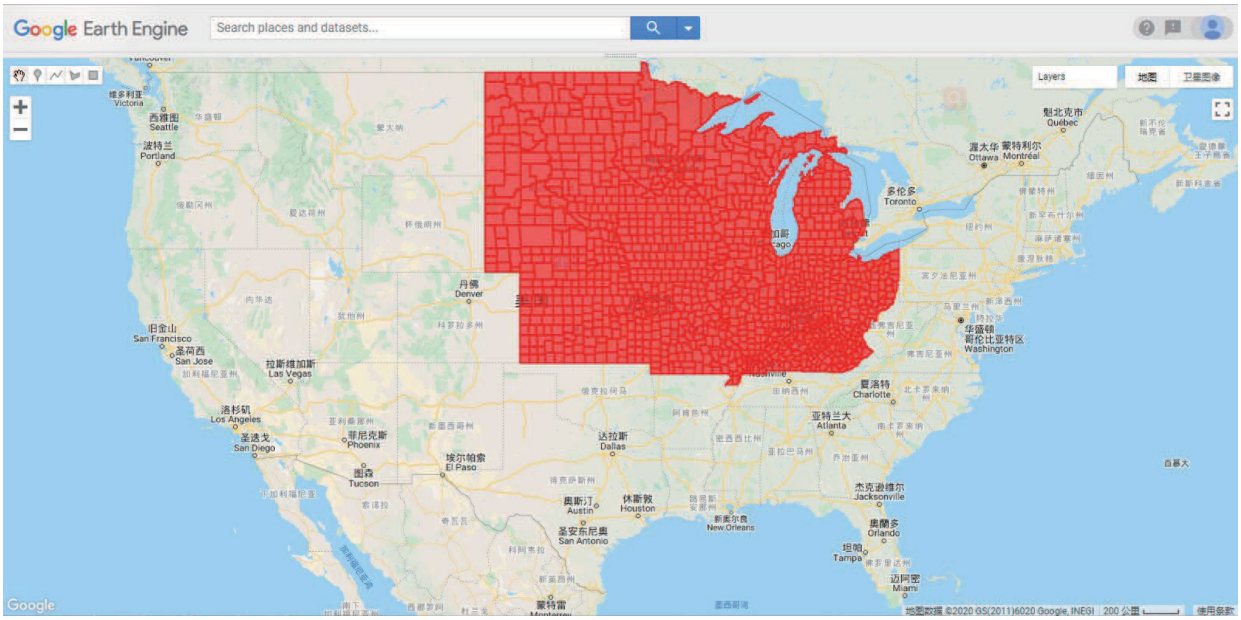

Fig. 1. Study area in the GEE editor (red areas show selected counties in the Corn Belt).

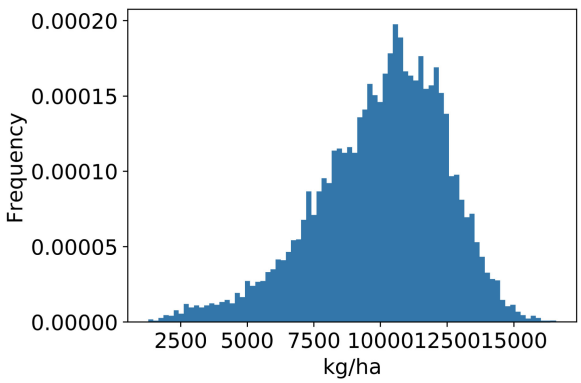

Fig. 2. Distribution of yields from 2007 to 2016.

including MODIS SR data; the other is environmental variables which consist of weather data, MODIS LST, and soil property. A long-term observation can promise mass data for DL, all the data and the corresponding yield data were collected from 2007 to 2016. Moreover, the study time window was set from April 1st to November 30th according to the Usual Planting and Harvesting Dates (UPHD) of U.S. corn [32]. All the data can be freely accessed in the GEE. The details are shown below.

1) USDA Yield Data: The county-level corn yield data from 2007 to 2016 were collected from the United States Department of Agriculture (USDA) Quick Stats [33]. The data were based on two large panel surveys conducted by the National Agricultural Statistics Service (NASS) and established by the NASS Agricultural Statistics Board. Fig. 2 shows the distribution of the corn yield at the county-level from 2007 to 2016, 11 339 records in total. The yield ranges from 1277.77 to 16590.79 kg/ha with a mean of 10016.63 kg/ha. The yield data were used as label data in the DL.

2) USDA NASS Cropland Data Layers (CDL): The Cropland Data Layer, hosted on CropScape, provides an annual raster, geo-referenced, crop-specific land cover map for the continental United States at 30 m spatial resolution. With the help of CDL, we can only focus on the corn data [34].

3) MODIS SR: Instead of directly using the handcraft VI, MODIS SR product (MOD09A1) which provides an estimate of the surface spectral reflectance was selected to reflect the state of crop growth. The MOD09A1, with bands 1–7, is a 500 m gridded, an 8-d composite product derived from the MODIS-Terra top of atmosphere reflectance swaths [35], [36].

4) MODIS LST: The MODIS LST products are composed of data from the daily 1 km LST product (MOD11A1) stored on a 1 km grid as the average values of clear sky LSTs during 8 d. MOD11A2 is comprised of daytime and nighttime LSTs, quality assurance assessment, observation times, view angles, bits of clear sky days and nights [37].

5) Weather Data: The Daymet dataset provides gridded estimates of daily weather parameters. Seven surface weather parameters are available at a daily time step, 1 km spatial resolution, with a North American spatial extent. It is derived from selected meteorological station data and various supporting data sources. In the study, two important weather parameters, precipitation, and vapor pressure were selected as climatic factors [38].

6) Soil Property Data: The GEE provides global predictions for standard numeric soil physical and chemical properties at six standard depths (0, 10, 30, 60, 100, and 200 cm) in GEE. The predictions were based on ca. 150 000 soil profiles used for training and a stack of 158 remote sensing-based soil covariates (primarily derived from MODIS land products, SRTM DEM derivatives, climatic images, and global landform and lithology maps) [39]. As shown in Table I, six important properties were selected as soil property data.

TABLE I
SOIL PROPERTIES SELECTED IN THE MODEL

Feature	Unit
Clay content mass fraction(CLAY)	%
Sand content mass fraction(SAND)	%
Water content at 33kPa(WATER)	%
pH in H2O(PH)	-
Bulk density(BULK)	kg/m^3
Carbon content(CARBON)	g/kg

C. GEE-Based Tensor Generation

Tensor generation is the key step for DL. Considering the efficiency of the DL, a dimension reduction was always conducted at first, for instance, most of the previous studies often use the averages of regions to simplify the raw data. However, DL prefers to learn the features from the raw data. Given the assumption that the position information of pixels is unimportant for yield prediction. Then, there is little loss of information in transforming the high-dimensional image into a histogram of pixel count. It is easy to reconstruct the histogram into a tensor for the DL. The histogram-based transformation can not only keep features as much as possible from the raw data but also decrease the dimension sharply. Thanks for the great computing power of GEE [40], the processing can be performed very efficiently over the U.S. Corn Belt. The key steps are as follows.

1) Preprocessing: All the data should be collected and cloud masked in the GEE. As for the time-series data, the daily weather data should be aligned to the 8-d MODIS data by the average values. The time-series data has 30 time steps during the whole growing season at an 8-d interval. Then, after combining the boundary data, each county will have a 11 bands image composite $M^t_{id,y}$ for time-series data at the tth ($0 < t \leq 30$) time step and a 36 bands S_{id} for constant soil property data in each year. The id represents the GEOID of a county and the y denotes a year in the list ranging from the start to the predicted year y'. The 11 bands of $M^t_{id,y}$ consists of 7 bands of the MODIS SR, 2 bands of the MODIS LST, and 2 bands of the weather data. The 36 bands of the S_{id} include 6 types of properties at 6 depths. The CDL data was employed to mask all noncorn pixels for all data.

2) Histogram-Based Tensor Generation: As the inputs of the DL, tensors always need regular shape. Our tensors come from the fixed-bins histogram-based transformation performed on the composites. Each band of composites over a county can be transformed into a histogram with n bins (the n was set to 32 for regulation in the study). Then, the $M^t_{id,y}$ can be transformed into the tensor $TM^t_{id,y} \in \mathbb{R}^{1\times 32\times 11}$, and the S_{id} will become the tensor $TS_{id} \in \mathbb{R}^{1\times 32\times 36}$. Finally, each county will have a yield label from USDA statistics, if any. For example, the tensors $TM^{18}_{20115,2016}$ and TS_{20115} of Kansas Marion county (GEOID:20115) in 2016 are visualized in Figs. A1 and A2 of Appendix IV. The *x*-axis represents the bin number (32) and the *y*-axis shows the normalized pixel count. The pixels of each band were distributed into 32 uniform bins according to the DN value.

D. Proposed DL Architecture

Fig. 3 shows the workflow of the prediction. The proposed DL architecture mainly consists of two modules. The first includes two levels for spatial and temporal feature extraction from time-series tensors. The other module is for soil property feature extraction from constant soil tensors. The output is the predicted yield. The detailed descriptions of each level are as follows.

1) Level I CNN for Time-Series Data: The time-series data include crop phenology and climate information. To explore more spatial features, a CNN method was proposed. As shown in Fig. 3, at each time step, the $TM^t_{id,y}$ was fed into the CNNs with K (k=2) 2-D convolution (Conv2D) layers. The output $TM^{t,K}_{id,y}$ from the Kth convolution layer can be defined in

$$TM^{t,K}_{id,y} = f(TM^{t,K-1}_{id,y} * W^K + B^K) \tag{1}$$

where $*$ represents the convolutional operation and f() is an activation function. The $TM^{t,K-1}_{id,y}$ is the output from the $(K-1)$th layer. W^K and B^K are parameters of the kth convolution layer.

Each convolution layer is followed by a batch normalization layer, which is used to normalize the input layer by adjusting and scaling the activations for improving the speed, performance, and stability of the networks [41]. After the batch normalization layer, the output is flattened into a long vector, which is sent into a fully connected (FC) layer. The FC offers learns features from all the combinations of the features of the previous layer. Finally, we can obtain a processed feature $VM^t_{id,y}$.

2) Level II LSTM for Time-Series Data: The relations of the time-series crop phenologies and climate changes are of significance for yield estimation. The LSTM, a special RNN which can solve the vanishing gradient problem, was employed for time-series feature analysis, as it is capable of learning long-term dependencies. The employed LSTM consists of the cell $c_t \in \mathbb{R}^h$ (the memory part of the LSTM unit) which contains h LSTM unit's cells at t interval, the input gate $i_t \in \mathbb{R}^h$, the output gate $o_t \in \mathbb{R}^h$, and the forget gate $f_t \in \mathbb{R}^h$. Intuitively, the cell can keep track of the dependencies of the input sequence. The input gate controls the extent of the new inputs, the forget gate controls the extent to which a value remains in the cell, and the output gate controls the extent to which the value in the cell is used to compute the output activation of the LSTM unit. The time-series output of level 1 is the input of the LSTM, the whole processing can be defined in

$$\begin{aligned} f_t &= \sigma(W_f x_t + U_f h_{t-1} + b_f) \\ i_t &= \sigma(W_i x_t + U_i h_{t-1} + b_i) \\ o_t &= \sigma(W_o x_t + U_o h_{t-1} + b_o) \\ c_t &= f_t \circ c_{t-1} + i_t \circ \sigma(W_c x_t + U_c h_{t-1} + b_c) \\ h_t &= o_t \circ \sigma(c_t) \end{aligned} \tag{2}$$

where the operator $\circ$ denotes the Hadamard product, the σ is the activation function, the $x_t \in \mathbb{R}^d$ is the input vector to the LSTM unit, the $h_t \in \mathbb{R}^h$ is the hidden state vector, the $W \in \mathbb{R}^{h\times d}$, $U \in \mathbb{R}^{h\times h}$, and $b \in \mathbb{R}^h$ are weight matrices and bias vector parameters that need to be learned during training. The

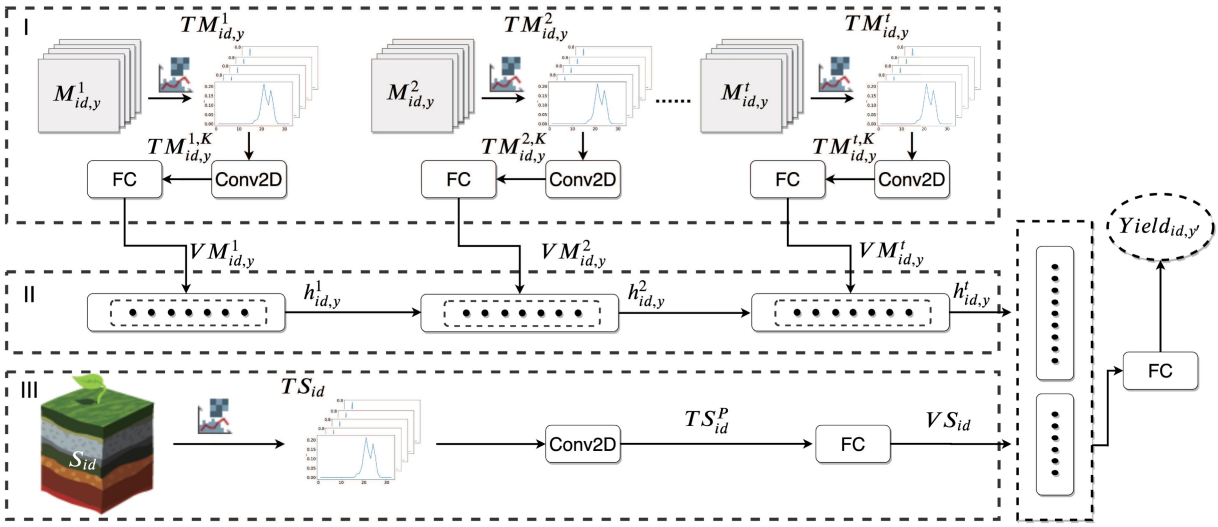

Fig. 3. Architecture of the MLDL-Net. The inputs are the time-series $TM^t_{id,y} \in \mathbb{R}^{1\times32\times11}$ tensors and constant $TS_{id} \in \mathbb{R}^{1\times32\times36}$ tensors. The output is the predicted yield $yield_{id,y'}$. Level I employs CNN networks for time-series data spatial features exploration at each time step, the CNN network consists of K Conv2D which followed by batch normalization layers and fully connected layers; Level II uses an LSTM network to explore the time-series features; Level III also uses CNN networks which can extract spatial features from soil property data. The output of Level II and Level III was flattened and concatenated into a vector. Finally, the vector was fed into the fully connected layer used for estimation.

superscripts d and h refer to the number of the input features and the hidden units, respectively.

3) Level III CNN for Soil Properties Data: Compared with the time-series data, the soil data of each pixel is constant. To capture the soil property features from the tensor TS_{id}, a CNN-based network was designed, which is similar to level 1. The network consists of P Conv2D layers and each layer is followed by a batch normalization layer. Therefore, the output of the Pth can be defined in (3). At last, all the features was flattened and fed into the FC layer

$$TS^P_{id} = f(TS^{P-1}_{id} * W^P + B^P) \tag{3}$$

where the TS^{P-1}_{id} is the output from the $(P-1)$th layer. W^P and B^P are parameters of the Pth convolution layer.

At the end of the workflow in Fig. 3, the output of level 2 and level 3 was concatenated together and fed into a dropout layer; the dropout layer can help prevent the model from overfitting [42]. Finally, an FC with only one unit is used to output the predicted yield $yield_{id,y'}$ of the predicted year y'.

4) Model Hyperparameter Tuning: The MLDL-Net includes several important hyperparameters, such as the number of Conv2D layers, the number of units, and the activation function, etc. For each hyperparameter, the range of possible values was defined as follows—layer_number = [2, 3, 4], unit_number = [32, 64, 128, 256], filter_number = [8, 16, 32], kernel_size = [1*2, 1*3], optimizer = ["SGD," "RMSprop," "Adam"], activation = ["ReLU," "Tanh," "Sigmoid"] [43]. Then the random search was performed on the parameter dictionary to find a tuple of hyperparameters that yields an optimal model that minimizes a predefined loss function. The mean squared error (MSE) was used as the loss metric.

E. Model Training and Evaluation

1) Model Training: More training data can provide a more stable result, to predict the $yield_{id,y'}$ of the target year y', all the $M^t_{id,y}$ and S_{id} was collected as the training data, where y ranges from 2007 to y', and the time steps t ranges from 0 to 30. Specifically, when $t = 30$, the model is identified for an after-season prediction, otherwise, it is for in-season prediction. In the study, 14 typical time nodes ranging from May 9th to November 25th were selected to explore the potential of the MLDL for in-season and after-season yield prediction. These time nodes mainly concentrate in June, July, and August, from which we hope to find out an in-season time node for a comparable performance of estimation. To ensure unbiasedness, a fixed ratio (0.3) of the training data were randomly separated for validation. During the training, the number of the epochs was set to 200 with a batch size of 16, however, too many epochs may lead to overfitting of the training dataset, and too few may result in an under-fit model. The mean absolute error was selected for a performance measure to monitor early stopping, which was employed as it can stop training once the model performance stops improving after ten consecutive epochs.

2) Model Evaluation: To evaluate the performance of the model, the target year y' of yield prediction was set to the value from 2013 to 2016 for an average evaluation. The number of training and test data is shown in Table II. Root RMSE and mean absolute percentage error (MAPE) were selected for overall evaluation measures, percent error (PE) was used for the distribution of the error map. Formulas of RMSE, MAPE, and PE are presented in (4)–(6) where x_i is the predicted value, $\hat{x}_i$ is the observed value, and n is the number of samples. Besides, the R^2 was also used to evaluate how well the predicted values

TABLE II
NUMBER OF THE TRAINING AND TEST DATA (2013–2016)

Year	Training	Test
2013	5863	915
2014	6778	935
2015	7713	875
2016	8588	913

can reconstruct the spatial variations of observed yield.

$$RMSE = \sqrt{\frac{\sum_{i=1}^{n}(x_i - \hat{x}_i)^2}{n}} \tag{4}$$

$$MAPE = \sum_{i=1}^{n}\left|\frac{x_i - \hat{x}_i}{\hat{x}_i}\right| \cdot \frac{100\%}{n} \tag{5}$$

$$PE = \frac{|x_i - \hat{x}_i|}{\hat{x}_i} \cdot 100\%. \tag{6}$$

3) Comparison With Baseline: To evaluate the performance of the proposed method, several state-of-the-art methods were employed as the baseline for comparison. These methods include least absolute shrinkage and selection operator (LASSO), ridge regression [44], RF [45], and a DNN with three hidden layers of 256 neurons each [46]. For fair comparisons, all methods use the same input data.

4) Comparison With Variants: All the input employed in the study can be divided into phenological data and environmental data, furthermore, the environmental data can fall into time-series and constant data in terms of the cadences. To analyze the influence of different input, several variants of the proposed method were compared as follows.

1) MLDL_SR: This model only uses the level I and II networks with MODIS SR data. This model was used to test the capacity of the phenological information for yield estimation.
2) MLDL_SR&ENV: This model uses the level I and II networks and excludes soil data. The model can show the influence of the soil data in the estimation.
3) MLDL_ENV: This model uses the three levels of networks and excludes MODIS SR data. The model was used to verify the contribution of the environmental data in the estimation.
4) MLDL Net: This is our proposed method combining all the data.

III. RESULTS AND DISCUSSION

1) Optimized Model Hyperparameters: Based on the MLDL, the hyperparameter optimization was carried out. The optimal number of Conv2D layers K and P were both set to 2, the filter number of Conv2D was set to 32, and the kernel size was set to 1*3. The activation function for all Conv2D was ReLU, and for LSTM was Tanh. The unit number of LSTM was set to 256. Besides, Adam was the best optimization function.

2) Performance Comparison With Baselines: Fig. 4 shows the performance of different models measured in RMSE, MAPE, and R^2. All the models have a similar pattern. None of the models

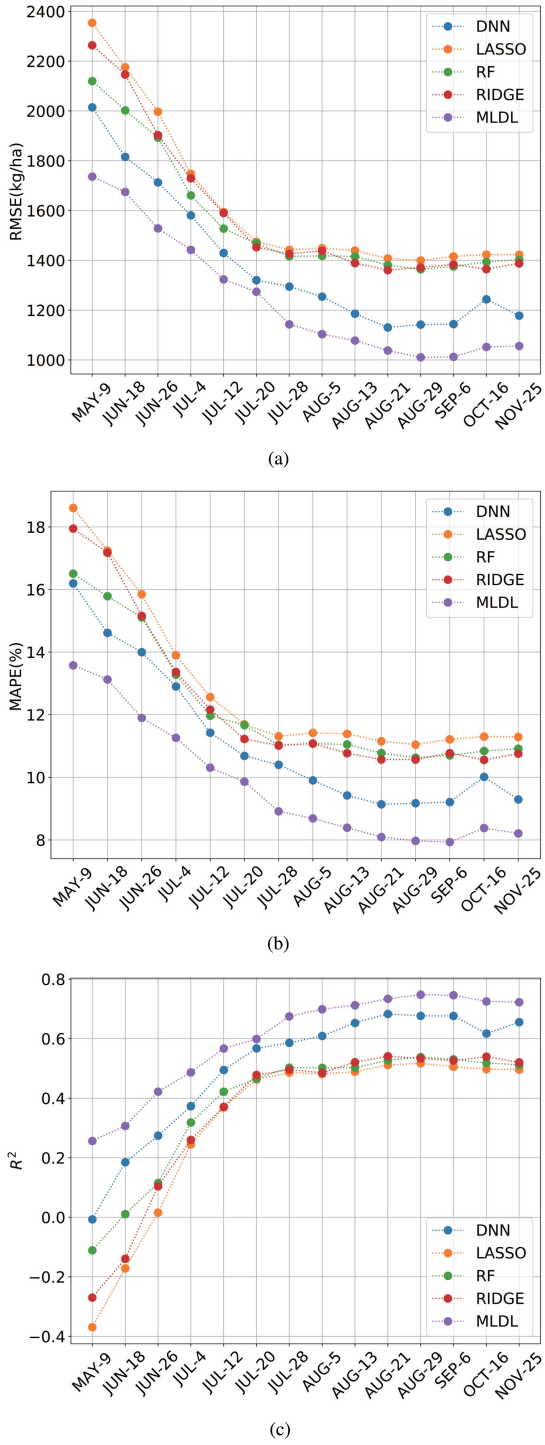

Fig. 4. Performance comparison with baselines at each selected time step measured in (a) RMSE, (b) MAPE, and (c) R^2.

can obtain a good result on May 9th, which suggests that it is difficult for yield estimation at the early crop growth stage such as the seedling stage or earlier. However, the performance of all models increases rapidly from May 9th to July 28th. The result indicates that the information on the jointing-booting stage is important for corn yield estimation. Furthermore, their performance improves relatively slowly from July 28th to November

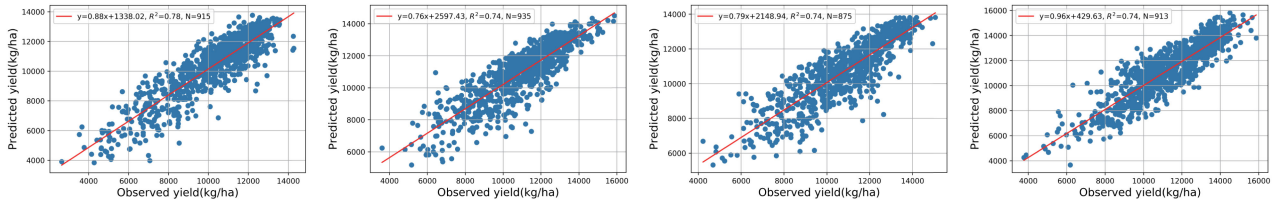

Fig. 5. Scatter plots of MLDL predicted versus observed yield on August 29th of (a) 2013, (b) 2014, (c) 2015, and (d) 2016.

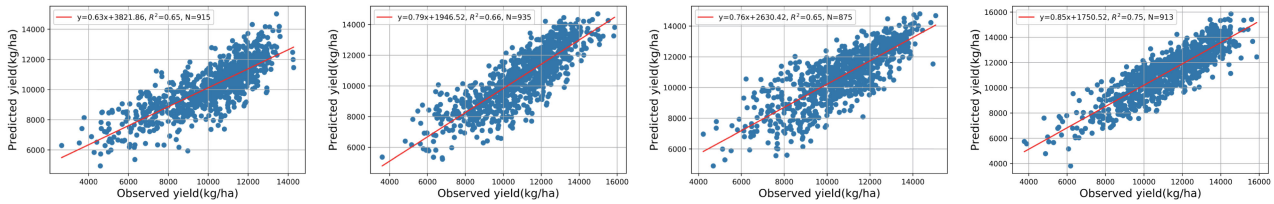

Fig. 6. Scatter plots of DNN predicted versus observed yield on Aug 29th of (a) 2013, (b) 2014, (c) 2015, and (d) 2016.

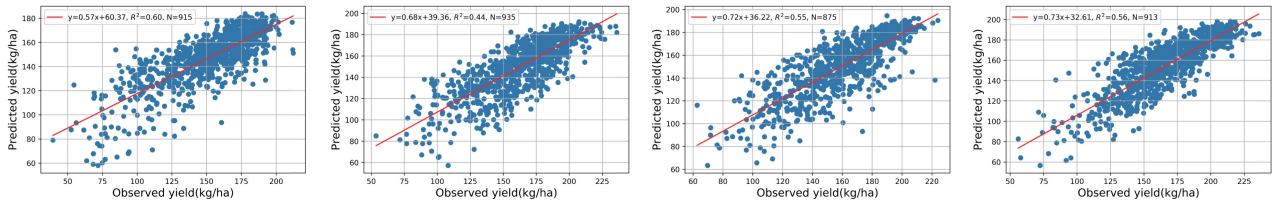

Fig. 7. Scatter plots of RF predicted versus observed yield on Aug 29th of (a) 2013, (b) 2014, (c) 2015, and (d) 2016.

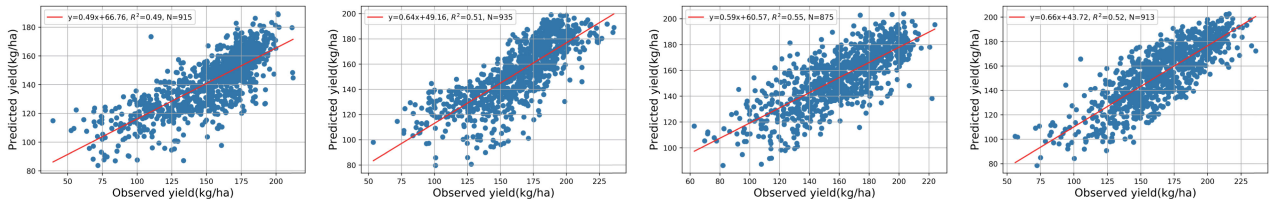

Fig. 8. Scatter plots of LASSO predicted versus observed yield on Aug 29th of (a) 2013, (b) 2014, (c) 2015, and (d) 2016.

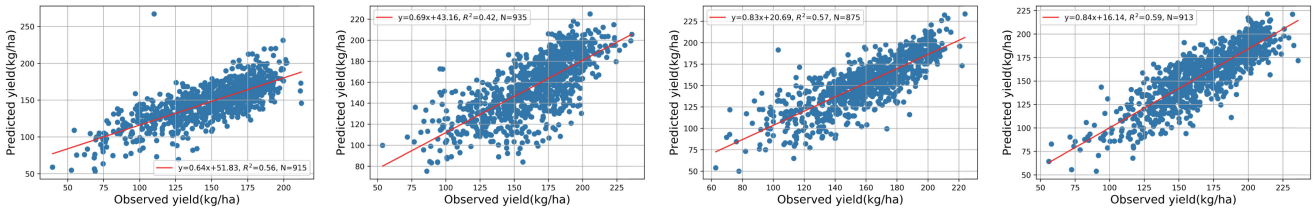

Fig. 9. Scatter plots of RIDGE predicted versus observed yield on Aug 29th of (a) 2013, (b) 2014, (c) 2015, and (d) 2016.

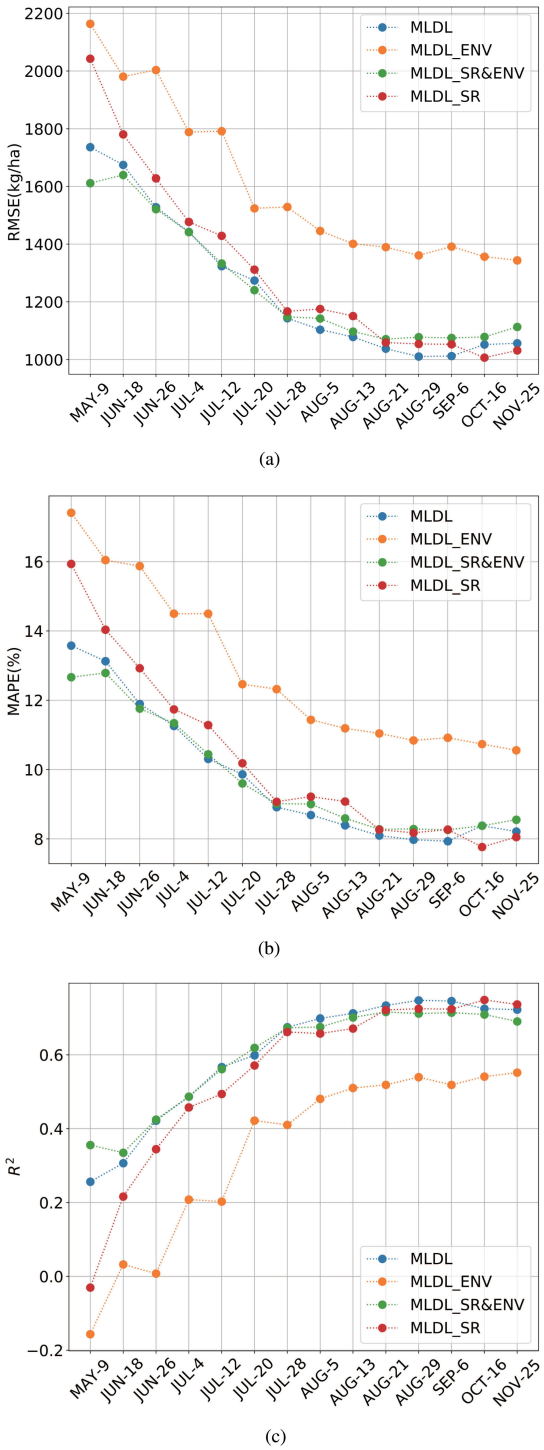

Fig. 10. Performance comparison with variants at each selected time step measured in (a) RMSE, (b) MAPE, and (c) R^2.

25th, and the best results of the models always occur between August 21st and September 6th, then the performance goes into a steady state with small fluctuation. It can be concluded that more information regarding crop can contribute to better performance, but the improvement is limited and unstable at the end of the season, the reason may be caused by different harvesting date in different states, for example, the information collected in some early harvesting states after October cannot represent the crop growth status precisely.

Meanwhile, the results also show that the DL methods (DNN and MLDL) can significantly outperform the traditional ML methods at each time node. Specifically, the DNN method achieves its best performance on August 21st with RMSE of 1130.44, MAPE of 9.14%, and R^2 of 0.68; and the MLDL Net has the best results among all the methods. The best performance of the MLDL Net always occurs on August 29th with the RMSE of 1010.61, MAPE of 7.97%, and R^2 of 0.75 which is about 21% improvement over the traditional baselines. Fig. 5 shows the scatter plots of MLDL predicted yield versus observed yield on August 29th from 2013 to 2016. As a comparison, Figs. 6–9 (DNN, RF, LASSO, and RIDGE) show the scatter plots of the baseline on the same day. The results indicate that DL methods can learn the relation between the features and the yield much better. Moreover, with the help of the proposed model, it is possible to make a satisfying early in-season yield prediction based on the proposed MLDL Net.

3) Performance Comparison With Variants: Fig. 10 shows the performance of different variants measured in RMSE, MAPE, and R^2. The performance of the variants is gradually improved over time, and most variants can achieve their best result between August 21st and September 6th, which is consistent with the result of MLDL in the above section. The scatter plots of the variants on August 29th are shown in Figs. 11–13. Generally, the proposed MLDL shows the best performance among the other variants, and the best accuracy of the MLDL always occurs on August 29th, by contrast, the MLDL_SR can achieve a comparable result, but 18 days late. Moreover, the MLDL_ENV model shows relatively poor accuracy compared with the MLDL_SR model at each time step, indicating that the phenological factors play more important roles than climate factors in the estimation. For which, there are several possible reasons. First, the crop yield is affected by a complex composition of external factors including but not limited to climate, irrigation policy, soil property, pests, and diseases. It is difficult to obtain a satisfying yield estimation result relying only on partial environmental data selected in the study. Second, in contrast to external factors, phenological factors can reflect the crop growth status more directly.

Meanwhile, the MLDL_SR&ENV model can outperform the MLDL_SR model before August 21st, but the superiority can not continue at the end of the season. The result indicates that the performance of the MLDL_SR model can be improved after environmental information added at the early-mid growth stage, but the improvement can not continue at the end of the season, in other words, the environmental data has relatively low influence for yield estimation at the end of the season. As the response of the crop phenological data is always later than the occurrence of environmental data, for instance, the MLDL_SR&ENV model can obtain the performance on July 28th with RMSE of 1148.07, MAPE of 9.02, and R^2 of 0.68, by contrast, the MLDL_SR model can just achieve a comparable result on August 13th, about 15 days late.

Furthermore, Fig. 14 also shows the proposed MLDL Net can outperform the MLDL_SR&ENV model slightly at the most

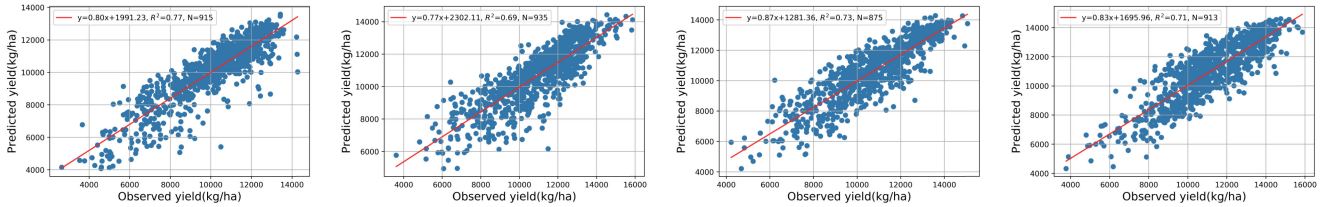

Fig. 11. Scatter plots of MLDL_SR&ENV predicted versus observed yield on Aug 29th of (a) 2013, (b) 2014, (c) 2015, and (d) 2016.

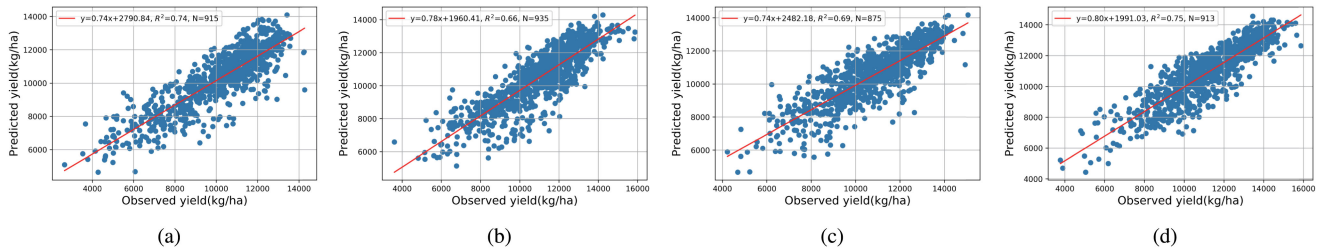

Fig. 12. Scatter plots of MLDL_SR predicted versus observed yield on Aug 29th of (a) 2013, (b) 2014, (c) 2015, and (d) 2016.

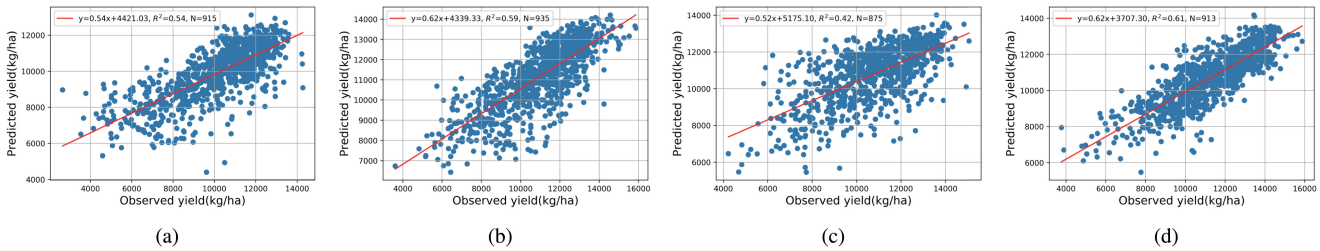

Fig. 13. Scatter plots of MLDL_ENV predicted versus observed yield on Aug 29th of (a) 2013, (b) 2014, (c) 2015, and (d) 2016.

time nodes, verifying the effectiveness of the soil property data for yield estimation.

4) Spatial Distribution of the Estimation Error: The estimation error map can help us figure out the performance of the model on a small spatial scale, which is useful to the model improvement in the future. As the MLDL has shown its superiority for in-season yield estimation, the results of the MLDL on August 29th were analyzed in the section. Fig. 14 shows the detailed comparison of the yield distribution map between the USDA yield data and the estimated yield in Corn Belt at the county-level by MLDL on August 29th. The first row is USDA corn yield data from 2013 to 2016, and the second row is the corresponding in-season estimated yield based on the proposed MLDL model. Besides, based on (6), the third row illustrates the estimation accuracy of each county measured in PE. The result shows high consistency between the estimated yield and the USDA yield, and most of the error can fall into the range from 0%–10%, these errors always occur in the center of the Corn Belt. However, there are still relatively large errors that always happen in a few states, such as North Dakota, South Dakota, Kansas, Missouri, and Indiana. The comparison shows that the counties with low estimation accuracy always share abnormal yield or abrupt yield changes in common. For which, the main possible reasons are: first, to build a strong estimation network, the DL method makes high demand on sample quantity and diversity, but the counties with abnormal yield only account for a small portion of the total samples, leading to inadequate learning; second, except for the selected predictors in the study, the crop yield can be affected by many other factors such as pests, varieties, extreme weather, and management quality, etc. [13], [22], [47], which are not considered in the study.

5) Influence of the Bin Numbers: This work transformed the natural remote sensing data into fixed-bins histograms as the inputs. To ascertain the influence of the bin numbers on the overall performance. Based on the MLDL, 16-bins and 64-bins tensor were added for comparison. Fig. A3, Fig. A1, and Fig. A4 show 16-bins, 32-bins, and 64-bins histogram-based tensors coming from the same remote sensing data, respectively. Compared with Fig. A3, Fig. A1 and Fig. A4 depict more details on the histograms but the shape of the distribution are essentially

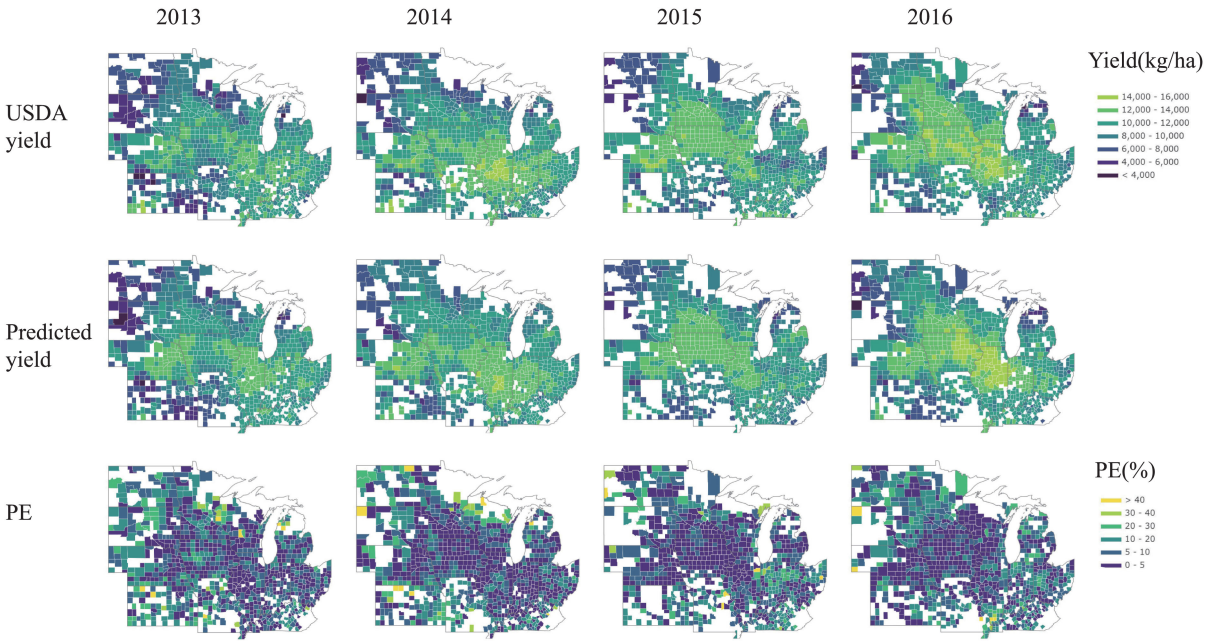

Fig. 14. Maps of MLDL in-season prediction and PE in different years.

TABLE III
MLDL PERFORMANCE COMPARISON WITH DIFFERENT BIN NUMBERS. A. IN SEASON. B. AFTER SEASON

Performance	16bins		32bins		64bins	
	a	b	a	b	a	b
R^2	0.73	0.75	0.75	0.72	0.75	0.73
RMSE(kg/ha)	1039.87	1008.93	1010.61	1056.51	1014.48	1038.69
MAPE(%)	8.11	7.84	7.97	8.21	7.93	8.22

uniform. By using the same MLDL model, the performance of these different tensors is shown in Table III. The performance was measured by R^2, RMSE, and MAPE which were all averaged from 2013 to 2016. The in-season results were evaluated on August 29th. With the increase of the bin number, there are no obvious improvements in the in-season and after-season results. A possible explanation is that the similarity between different fixed-bins histograms lead to similar performance, and the trivial difference can only play a minimal role in the task.

IV. CONCLUSION

Predicting crop yield is very important in agriculture management. Recent studies have proven remote sensing is an efficient method for yield estimation and ML, especially deep learning, can infer a good prediction by integrating multisource datasets such as satellite data, climate data, soil data, and so on. However, there are some bottleneck challenges to improve accuracy. The current deep learning for yield prediction cannot input benchmark data that labels the native properties such as soil properties. Meanwhile, both temporal and spatial features play a role in affecting the yields. But the existing approaches employed either CNN or RNN . CNN cannot learn temporal patterns, while RNN barely can learn spatial characteristics. This work proposed a novel multilevel deep learning model coupling RNN and CNN to extract both spatial and temporal features. The inputs include both time-series remote sensing data and soil property data and the model outputs yield. We experimented with the model in U.S. Corn Belt states and used it to predict corn yield from 2013 to 2016 at the county-level. The results approve the effectiveness and advantages of the proposed approach over the other methods.

Furthermore, to evaluate the influence of different data in the estimation framework, several variants employing different inputs were designed. The comparison suggests that the phenological factors play a more important role than the climate factor because the phenological factor can reflect the crop growth status more directly, besides, the performance can be improved when multifactors are integrated, but the improvement is limited.

The proposed model has no location-specific assumptions and should be able to be reused on other crops in other regions/countries. A few improvements are on our to-do list. Additional impact factors such as crop varieties, pests, disease, and extreme weather, etc., should be considered as well. Meanwhile, the architecture of the network should also be updated to make the method flexible to adapt with different vegetation index products of various time resolutions from various satellites.

APPENDIX A

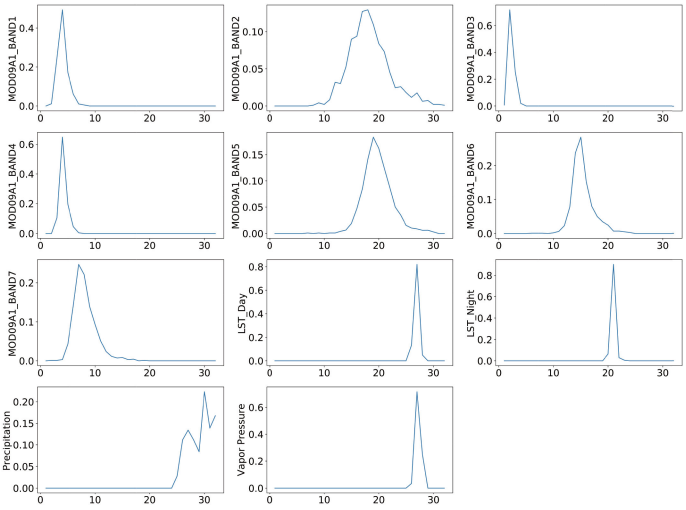

Fig. A1. 32-bins histogram-based tensors $TM^{18}_{20115,2016}$.

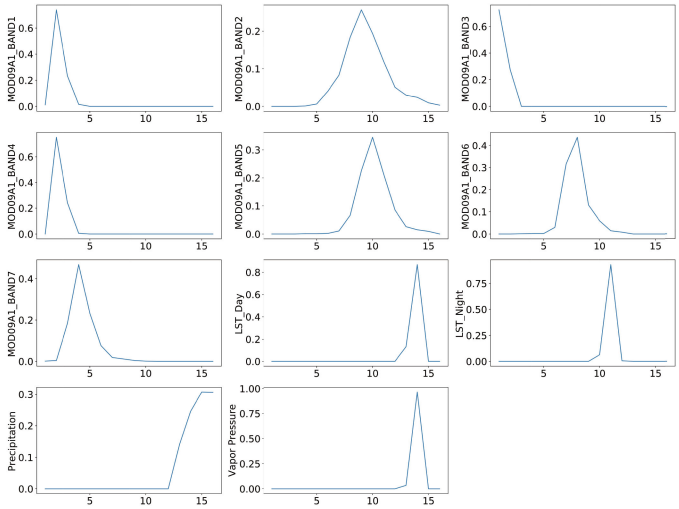

Fig. A3. 16-bins histogram-based tensors $TM^{18}_{20115,2016}$.

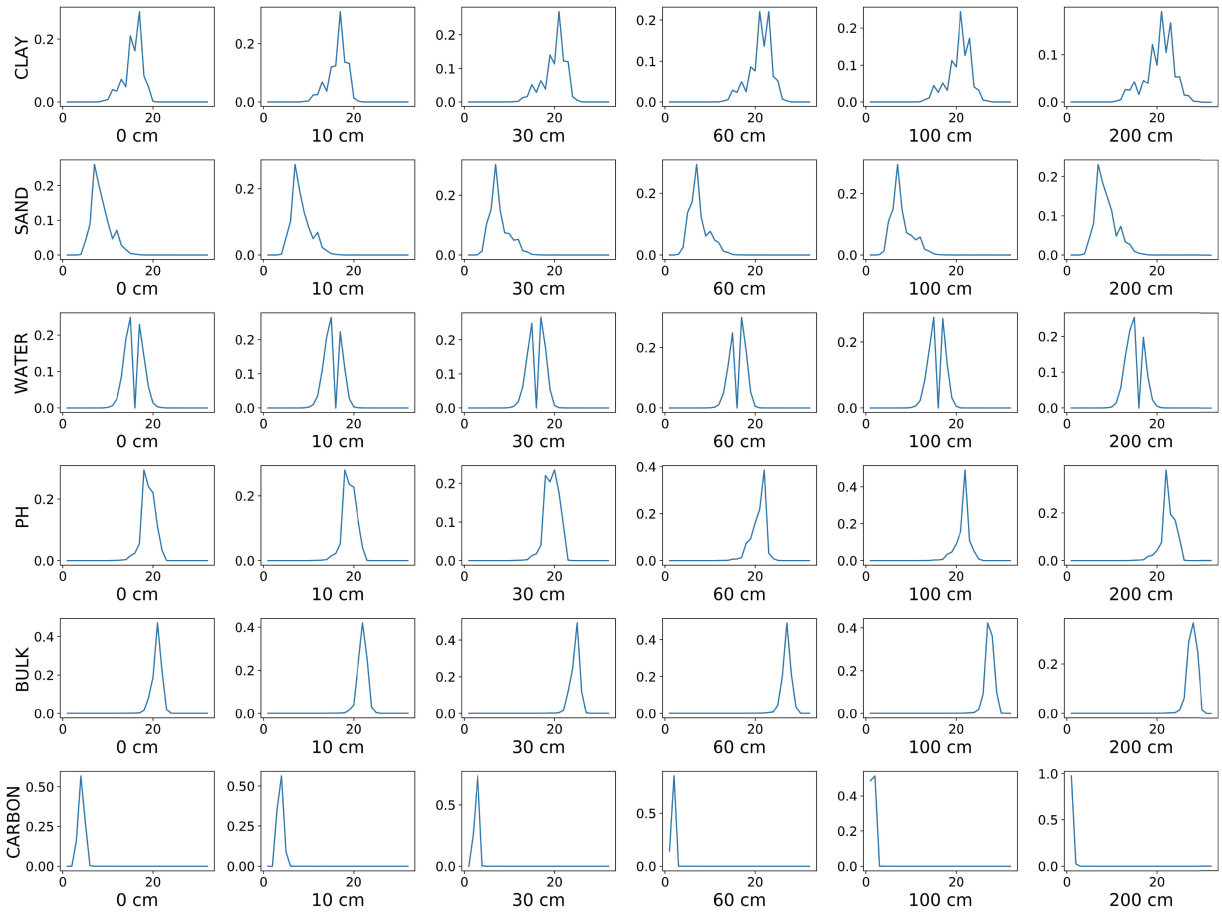

Fig. A2. 32-bins histogram-based tensors TS_{20115}.

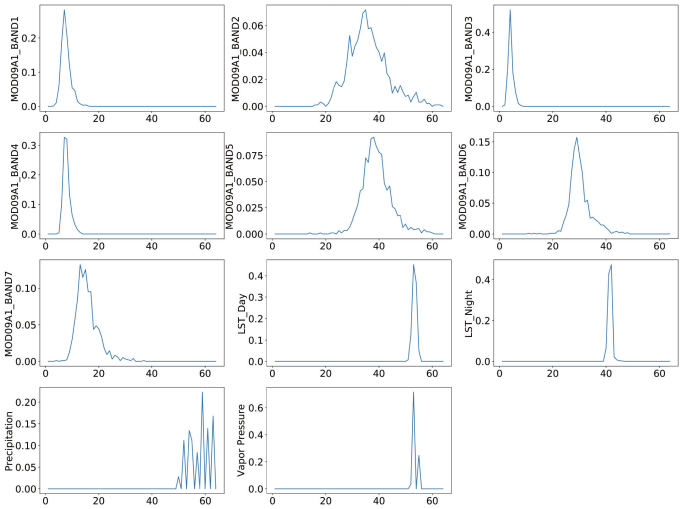

Fig. A4. 64-bins histogram-based tensors $TM^{18}_{20115,2016}$.

REFERENCES

[1] K. Akhand, M. Nizamuddin, L. Roytman, and F. Kogan, "Using remote sensing satellite data and artificial neural network for prediction of potato yield in Bangladesh," *Proc. SPIE*, vol. 9975, Sep. 19, 2016, Art. no. 997508.

[2] Z. Sun, L. Di, and H. Fang, "Using long short-term memory recurrent neural network in land cover classification on landsat and cropland data layer time series," *Int. J. Remote Sens.*, vol. 40, no. 2, pp. 593–614, 2019.

[3] J. Dong *et al.*, "Mapping paddy rice planting area in northeastern Asia with Landsat 8 images, phenology-based algorithm and Google Earth Engine," *RemoteSens. Environ.*, vol. 185, no. SI, pp. 142–154, Nov. 2016.

[4] C. Domenikiotis, M. Spiliotopoulos, E. Tsiros, and N. Dalezios, "Early cotton yield assessment by the use of the NOAA/AVHRR derived vegetation condition index (VCI) in Greece," *Int. J. Remote Sens*, vol. 25, no. 14, pp. 2807–2819, 2004.

[5] K. Akhand, M. Nizamuddin, L. Roytman, F. Kogan, and M. Goldberg, "Using artificial neural network and satellite data to predict rice yield in Bangladesh," *Proc. SPIE*, vol. 9610, Sep. 4, 2015, Art. no. 96100E.

[6] J.-W. Ma, C.-H. Nguyen, K. Lee, and J. Heo, "Regional-scale rice-yield estimation using stacked auto-encoder with climatic and MODIS data: A case study of South Korea," *Int. J. Remote Sens.*, vol. 40, no. 1, pp. 51–71, Jan. 2019.

[7] H.-Y. Ban, K. S. Kim, N.-W. Park, and B.-W. Lee, "Using MODIS data to predict regional corn yields," *Remote Sens.*, vol. 9, no. 1, Jan. 2017, Art. no. 16.

[8] M. Mkhabela, P. Bullock, S. Raj, S. Wang, and Y. Yang, "Crop yield forecasting on the Canadian prairies using modis NDVI data," *Agricultural Forest Meteorol.*, vol. 151, no. 3, pp. 385–393, 2011.

[9] S. Skakun, E. Vermote, J.-C. Roger, and B. Franch, "Combined use of Landsat-8 and Sentinel-2A images for winter crop mapping and winter wheat yield assessment at regional scale," *AIMS Geosci.*, vol. 3, no. 2, pp. 163–186, 2017.

[10] A. Haghverdi, R. A. Washington-Allen, and B. G. Leib, "Prediction of cotton lint yield from phenology of crop indices using artificial neural networks," *Comput. Electron. Agriculture*, vol. 152, pp. 186–197, Sep. 2018.

[11] J. L. Fernandes, N. F. Favilla Ebecken, and J. C. Dalla Mora Esquerdo, "Sugarcane yield prediction in Brazil using NDVI time series and neural networks ensemble," *Int. J. Remote Sens.*, vol. 38, no. 16, pp. 4631–4644, 2017.

[12] S. S. Panda, D. P. Ames, and S. Panigrahi, "Application of vegetation indices for agricultural crop yield prediction using neural network techniques," *Remote Sens.*, vol. 2, no. 3, pp. 673–696, 2010. [Online]. Available: https://www.mdpi.com/2072-4292/2/3/673

[13] B. Pourmohammadali, S. J. Hosseinifard, M. H. Salehi, H. Shirani, and I. E. Boroujeni, "Effects of soil properties, water quality and management practices on pistachio yield in Rafsanjan region, southeast of Iran," *plbibitalic-Agricultural Water Manage.*, vol. 213, pp. 894–902, Mar. 2019.

[14] Y. Cai *et al.*, "Integrating satellite and climate data to predict wheat yield in Australia using machine learning approaches," *Agricultural Forest Meteorol.*, vol. 274, pp. 144–159, Aug. 2019.

[15] K. Liakos, P. Busato, D. Moshou, S. Pearson, and D. Bochtis, "Machine learning in agriculture: A review," *Sensors*, vol. 18, no. 8, Aug. 2018, Art. no. 2674.

[16] A. Chlingaryan, S. Sukkarieh, and B. Whelan, "Machine learning approaches for crop yield prediction and nitrogen status estimation in precision agriculture: A review," *Comput. Electron. Agriculture*, vol. 151, pp. 61–69, Aug. 2018.

[17] Y. Everingham, J. Sexton, D. Skocaj, and G. Inman-Bamber, "Accurate prediction of sugarcane yield using a random forest algorithm," *Agronomy Sustain. Develop.*, vol. 36, no. 2, 2016, Art. no. 27.

[18] G. Ruß, "Data mining of agricultural yield data: A comparison of regression models," in *Proc. Ind. Conf. Data Mining*, 2009, pp. 24–37.

[19] A. J. Freitas Leal, E. P. Miguel, F. H. Rojo Baio, D. d. C. Neves, and U. A. Severino Leal, "Artificial neural networks for corn yield prediction and definition of site-specific crop management through soil properties," *Bragantia*, vol. 74, no. 4, pp. 436–444, Oct.-Dec. 2015.

[20] K. Matsumura, C. F. Gaitan, K. Sugimoto, A. J. Cannon, and W. W. Hsieh, "Maize yield forecasting by linear regression and artificial neural networks in Jilin, China," *J. Agricultural Sci*, vol. 153, no. 3, pp. 399–410, Apr. 2015.

[21] F. C. Soares, A. D. Robaina, M. X. Peiter, and J. L. Russi, "Corn crop production prediction using artificial neural network," *Ciencia Rural*, vol. 45, no. 11, pp. 1987–1993, Nov. 2015.

[22] Y. Yan, C.-C. Feng, M. P.-H. Wan, and K. T.-T. Chang, "Multiple regression and artificial neural network for the prediction of crop pest risks," in *Proc. Inf. Syst. or Crisis Response nd Manage. Mediterranean Countries*, 2015, pp. 73–84.

[23] M. Safa, S. Samarasinghe, and M. Nejat, "Prediction of wheat production using artificial neural networks and investigating indirect factors affecting it: Case study in Canterbury Province, New Zealand," *J. Agricultural Sci. Technol*, vol. 17, no. 4, pp. 791–803, Jul./Aug. 2015.

[24] N. Kim, K.-J. Ha, N.-W. Park, J. Cho, S. Hong, and Y.-W. Lee, "A comparison between major artificial intelligence models for crop yield prediction: Case study of the Midwestern United States, 2006–2015," *ISPRS Int. J. Geo-Inf.*, vol. 8, no. 5, 2019, Art. no. 240. [Online]. Available: https://www.mdpi.com/2220-9964/8/5/240

[25] S. Khaki and L. Wang, "Crop yield prediction using deep neural networks," *Frontiers Plant Sci.*, 2019, vol. 10, p. 621, [Online]. Available: https://doi.org/10.3389/fpls.2019.00621

[26] Y. LeCun, Y. Bengio, and G. Hinton, "Deep learning," *Nature*, vol. 521, no. 7553, pp. 436–444, 2015.

[27] Z. Jiang, C. Liu, N. P. Hendricks, B. Ganapathysubramanian, D. J. Hayes, and S. Sarkar, "Predicting county level corn yields using deep long short term memory models," 2018, *arXiv:1805.12044*.

[28] J. You, X. Li, M. Low, D. Lobell, and S. Ermon, "Deep Gaussian process for crop yield prediction based on remote sensing data," in *Proc. Assoc. Advancement Artif. Intell.*, Feb. 2017, pp. 4559–4566.

[29] A. X. Wang, C. Tran, N. Desai, D. Lobell, and S. Ermon, "Deep transfer learning for crop yield prediction with remote sensing data," in *Proc. 1st ACM SIGCAS Conf. Comput. Sustain. Soc.*, Jun. 2018, pp. 50:1–50:5. [Online]. Available: http://doi.acm.org/10.1145/3209811.3212707

[30] H. Russello, "Convolutional neural networks for crop yield prediction using satellite images," M.S. thesis, Dept., IBM Center Adv. Stud. Univ. Amsterdam, Amsterdam, The Netherlands, 2018.

[31] Q. Yang, L. Shi, J. Han, Y. Zha, and P. Zhu, "Deep convolutional neural networks for rice grain yield estimation at the ripening stage using UAV-based remotely sensed images," *Field Crops Res.*, vol. 235, pp. 142–153, Apr. 2019.

[32] USDA, "The USDA economics, statistics and market information system," Accessed: Sep. 19, 2019. [Online]. Available: https://usda.library.cornell.edu/?locale=en

[33] NASS, "USDA national agricultural statistics service," Accessed: Sep. 19, 2019. [Online]. Available: https://www.nass.usda.gov/Quick_Stats/index.php/

[34] USDA-NASS, "USDA national agricultural statistics service cropland data layer," Accessed: Sep. 19, 2019. [Online]. Available: https://nassgeodata.gmu.edu/CropScape

[35] E. Vermote, "MOD09A1 MODIS/Terra surface reflectance 8-day L3 global 500m SIN grid V006," NASA EOSDIS Land Processes DAAC, Sioux Falls, SD, USA, 2015, doi: 10.5067/MODIS/MOD09A1.006.

[36] H. Tang, K. Yu, O. Hagolle, K. Jiang, X. Geng, and Y. Zhao, "A cloud detection method based on a time series of modis surface reflectance images," *Int. J. Digit. Earth*, vol. 6, pp. 157–171, 2013. [Online]. Available: https://doi.org/10.1080/17538947.2013.833313

[37] Z. Wan, S. Hook, and G. Hulley, "MOD11A2 MODIS/Terra land surface temperature/emissivity 8-day L3 Global 1km SIN Grid V006," NASA EOSDIS Land Processes DAAC, Sioux Falls, SD, USA, 2015, doi: 10.5067/MODIS/MOD11A2.006.
[38] P. Thornton *et al.*, "Daymet: Daily surface weather data on a 1-km grid for North America, Version 3," ORNL DAAC, Oak Ridge, TN, USA, 2017, doi: 10.5067/MODIS/MOD11A2.006.
[39] T. Hengl *et al.*, "Soilgrids250m: Global gridded soil information based on machine learning," *PLOS ONE*, vol. 12, no. 2, pp. 1–40, 2017. [Online]. Available: https://doi.org/10.1371/journal.pone.0169748
[40] GEE, "Google Earth Engine," (2019). Accessed: Sep. 19, 2019. [Online]. Available: https://developers.google.com/earth-engine
[41] S. Ioffe and C. Szegedy, "Batch normalization: Accelerating deep network training by reducing internal covariate shift," in *Proc. 32nd Int. Conf. Mach. Learn.*, 2015, pp. 448–456.
[42] P. Baldi and P. J. Sadowski, "Understanding dropout," in *Advances in Neural Information Processing Systems*, C. J. C. Burges, L. Bottou, M. Welling, Z. Ghahramani, and K. Q. Weinberger, Eds. Red Hook, NY, USA: Curran Associates, Inc., 2013, pp. 2814–2822. [Online]. Available: http://papers.nips.cc/paper/4878-understanding-dropout.pdf
[43] A. Gulli and S. Pal, *Deep Learning With Keras*. Birmingham, U.K.: Packt Publishing Ltd., 2017.
[44] D. K. Bolton and M. A. Friedl, "Forecasting crop yield using remotely sensed vegetation indices and crop phenology metrics," *Agricultural Forest Meteorol.*, vol. 173, pp. 74–84, 2013. [Online]. Available: http://www.sciencedirect.com/science/article/pii/S0168192313000129
[45] Y. Cai *et al.*, "Integrating satellite and climate data to predict wheat yield in australia using machine learning approaches," *Agricultural orest Meteorol.*, vol. 274, pp. 144–159, 2019. [Online]. Available: http://www.sciencedirect.com/science/article/pii/S0168192319301224
[46] K. Kuwata and R. Shibasaki, "Estimating crop yields with deep learning and remotely sensed data," in *Proc. IEEE Int. Geosci. Remote Sens. Symp.*, Jul. 2015, pp. 858–861.
[47] A. Cogato, F. Meggio, M. Migliorati, and F. Marinello, "Extreme weather events in agriculture: A systematic review," *Sustainability*, vol. 11, 2019, Art. no. 2547.

Jie Sun received the Ph.D. degree in photogrammetry and remote sensing from the Faculty of Remote Sensing and Information Engineering, Wuhan University, Wuhan, China, in 2011.

Since 2011 he is a Lecturer with the China University of Geosciences, Wuhan, China. He has authored or coauthored more than 20 papers. His research interests include remote sensing application for geology, agriculture, and machine learning for object recognition.

Zulong Lai received the Ph.D degree in photogrammetry and remote sensing from Wuhan University, Wuhan, China, in 2011.

He is an Associate Professor, Master's Tutor with China University of Geosciences, Wuhan, China. His research interests include land monitoring, pattern recognition, and deformation monitoring.

Liping Di (Senior Member, IEEE) received the Ph.D. degree in remote sensing/GIS (geography) from the University of Nebraska–Lincoln, Lincoln, NE, USA, in 1991.

He is the Founding Director of the Center for Spatial Information Science and Systems, a University Research Center, George Mason University, Fairfax, VA, USA. He is also a Professor with the Department of Geography and Geoinformation Science, George Mason University. He has engaged in geoinformation science research for more than 30 years and has authored or coauthored more than 400 publications. His research interests include geospatial information standards, geospatial cyberinfrastructure, web-based geospatial information and knowledge systems, and geoinformation science applications, particularly in agriculture.

Dr. Di was the recipient of many prestigious awards, such as the Merit Award from International Committee on Information Technology Standards, the Honor Award from the Secretary of U.S. Department of Agriculture, and the R&D Award from the R&D Magazine. He has received more than $57 million research grants from U.S. federal agencies and international organizations as the Principal Investigator. He was the Chair of INCITS/L1, the U.S. national committee responsible for setting U.S. national standards on geographic information and representing the United States at the ISO Technical Committee 211 (ISO TC 211) from 2010 to 2016. He was also the Elected Chair of Data Archive and Distribution Technical Committee (which has been renamed to Earth Science Informatics Technical Committee) of the IEEE Geoscience and Remote Sensing Society from 2005 to 2009.

Ziheng Sun received the B.S. degree in geographic information system and the Ph.D. degree in photogrammetry and remote sensing from Wuhan University, Wuhan, China, in 2009 and 2015, respectively.

Since February 2013, he has been with the Center for Spatial Information Science and Systems, George Mason University, Fairfax, VA, USA, where he is currently working as a Research Assistant Professor. His research achievements include regular object similarity index, parameterless automatic classification, customized vegetation condition index, LSTM-aided crop mapping, web-based supervised classification system, and located-based service for on-site information access. His research interests include geospatial web services, workflow-based geospatial modeling, machine learning, remote sensing, agricultural land cover classification, and drought monitoring.

Jianbin Tao received the Ph.D. degree in photogrammetry and remote sensing from the Faculty of Remote Sensing and Information Engineering, Wuhan University, Wuhan, China.

He is currently an Associate Professor with the School of Urban and Environmental Sciences, Central China Normal University, Wuhan, China. His main research achievements include a hierarchical naive Bayesian network classifier embedded Gaussian mixture model for textural image, a Bayesian network model fusing prior knowledge (BNPK) model fusing regional differentiation factor as prior knowledge and its application to regional cropping intensity mapping. His research interests include land use/land cover change, vegetation dynamics, fine resolution crop mapping, cropping intensity, and multisource remote sensing data fusion based on Bayesian network.

Yonglin Shen received the B.S. degree in geographic information system from the Wuhan University of Technology, Wuhan, China, in 2016, the M.S. degree in cartography and geographic information system from Nanjing Normal University, Nanjing, China, in 2009, and the Ph.D. degree in cartography and geographic information system from Beijing Normal University, Beijing, China, in 2013. During 2011–2013, he studied with the Center for Spatial Information Science and Systems, George Mason University, Fairfax, VA, USA.

He is currently working as an Assistant Professor with the China University of Geosciences, Wuhan, China. His research interests include remote sensing, agricultural land cover classification, crop phenology, and drought monitoring.